Original Article | Cardiovascular Imaging

eISSN 2005-8330
https://doi.org/10.3348/kjr.2021.0050
Korean J Radiol 2021;22(11):1777-1785

Korean Journal of Radiology
KJR

Accurate Measurement of Agatston Score Using kVp-Independent Reconstruction Algorithm for Ultra-High-Pitch Sn150 kVp CT

Xi Hu[1], Xinwei Tao[2], Yueqiao Zhang[1], Zhongfeng Niu[1], Yong Zhang[1], Thomas Allmendinger[3], Yu Kuang[4], Bin Chen[1]

[1]Department of Radiology, Sir Run Run Shaw Hospital, Zhejiang University School of Medicine, Hangzhou, China; [2]Siemens Healthineers China, Shanghai, China; [3]Computed Tomography-Research & Development, Siemens Healthcare GmbH, Erlangen, Germany; [4]Medical Physics Program, University of Nevada, Las Vegas, NV, USA

Objective: To investigate the accuracy of the Agatston score obtained with the ultra-high-pitch (UHP) acquisition mode using tin-filter spectral shaping (Sn150 kVp) and a kVp-independent reconstruction algorithm to reduce the radiation dose.
Materials and Methods: This prospective study included 114 patients (mean ± standard deviation, 60.3 ± 9.8 years; 74 male) who underwent a standard 120 kVp scan and an additional UHP Sn150 kVp scan for coronary artery calcification scoring (CACS). These two datasets were reconstructed using a standard reconstruction algorithm (120 kVp + Qr36d, protocol A; Sn150 kVp + Qr36d, protocol B). In addition, the Sn150 kVp dataset was reconstructed using a kVp-independent reconstruction algorithm (Sn150 kVp + Sa36d, protocol C). The Agatston scores for protocols A and B, as well as protocols A and C, were compared. The agreement between the scores was assessed using the intraclass correlation coefficient (ICC) and the Bland–Altman plot. The radiation doses for the 120 kVp and UHP Sn150 kVp acquisition modes were also compared.
Results: No significant difference was observed in the Agatston score for protocols A (median, 63.05; interquartile range [IQR], 0–232.28) and C (median, 60.25; IQR, 0–195.20) ($p = 0.060$). The mean difference in the Agatston score for protocols A and C was relatively small (-7.82) and with the limits of agreement from -65.20 to 49.56 (ICC = 0.997). The Agatston score for protocol B (median, 34.85; IQR, 0–120.73) was significantly underestimated compared with that for protocol A ($p < 0.001$). The UHP Sn150 kVp mode facilitated an effective radiation dose reduction by approximately 30% (0.58 vs. 0.82 mSv, $p < 0.001$) from that associated with the standard 120 kVp mode.
Conclusion: The Agatston scores for CACS with the UHP Sn150 kVp mode with a kVp-independent reconstruction algorithm and the standard 120 kVp demonstrated excellent agreement with a small mean difference and narrow agreement limits. The UHP Sn150 kVp mode allowed a significant reduction in the radiation dose.
Keywords: *Dual-source CT; Coronary artery calcium; Agatston score; Radiation dose*

INTRODUCTION

The coronary artery calcification scoring (CACS) system has been used as a critical tool for cardiovascular risk assessment and patient management since its introduction in the 1990s [1]. It represents calcific atherosclerosis in

Received: January 20, 2021 **Revised:** June 9, 2021 **Accepted:** June 12, 2021
The authors gratefully acknowledge the supports by the Medical Health Science and Technology Project of Zhejiang Provincial Health Commission under Grant numbers 2021RC071.
Corresponding author: Bin Chen, MD, Department of Radiology, Sir Run Run Shaw Hospital, Zhejiang University School of Medicine, 3 East Qingchun Road, Hangzhou, Zhejiang 310010, China.
• E-mail: chenbin50061@zju.edu.cn; and
Yu Kuang, PhD, Medical Physics Program, University of Nevada, 4505 S Maryland Pkwy, Las Vegas, NV 89121, USA.
• E-mail: yu.kuang@unlv.edu

the coronary arteries and is associated with the overall burden of coronary atherosclerosis. Moreover, it has been proven to be superior to risk scores or cardiac biomarkers for identifying those individuals who would benefit from primary prevention of cardiovascular disease [2-4].

According to the Society of Cardiovascular Computed Tomography (CT) guidelines, CACS is performed using a multidetector CT scanner with sequential acquisition and a standard fixed tube voltage of 120 kVp [5]. With the increasing interest in reducing the radiation dose, some investigations have been conducted in this field for CACS scans, including tube voltage reduction [6], tube current reduction, and spectral shaping with tin-filter techniques [7,8]. Although reducing the tube voltage results in a partial decrease in the radiation dose, the image artifacts and CT value changes during the process limit the application of this method [9]. Tin filter technology eliminates low-voltage electrons and modifies X-ray spectra, which facilitated a significant dose reduction in previous studies [10-12]. However, this method may change the CT value of the images and require a shift in the threshold for calcium scoring [11]. The ultra-high-pitch (UHP) mode using dual-source CT (DSCT) can reduce respiratory motion artifacts in CT images, which benefit patients who are incapable of holding their breath, and further reduce the radiation dose. However, due to the speed of the table movement, derived measurements could substantially result in different Agatston scores [10,13,14].

A novel kVp-independent reconstruction algorithm was introduced by Siemens Healthineers to adapt the Agatston score to different tube voltages. The accuracy of this algorithm has been validated using sequential modes at Sn100 kVp and patient-adapted tube voltages in previous studies [15,16]. In this study, we sought to extend the algorithm to validate the Agatston score accuracy using the UHP scan mode. To the best of our knowledge, this is the first study to investigate the accuracy of the Agatston score under UHP modes.

This study aimed to investigate the accuracy of the Agatston score obtained with the UHP Sn150 kVp acquisition mode and a kVp-independent reconstruction algorithm to reduce the radiation dose.

MATERIALS AND METHODS

Study Population

A total of 120 clinically indicated patients underwent prospective electrocardiogram (ECG)-triggered CACS using the standard 120 kVp acquisition mode, followed by an additional UHP Sn150 kVp scan between June and August 2020. Four patients with prior percutaneous stent implantation were excluded from this study. To ensure UHP image quality, two patients with a heart rate of > 75 bpm were also excluded. Therefore, a total of 114 patients (mean age ± standard deviation, 60.3 ± 9.8 years, 74 male) were enrolled in this prospective single-center study. The local Institutional Review Board approved our study, and written informed consent was obtained from all the patients (IRB No. 20200619-33).

CT Image Acquisitions and Image Reconstructions

The CT images were acquired using a third-generation DSCT system (SOMATOM Force, Siemens Healthcare) with two different acquisition parameters.

1) A standard sequential acquisition with prospective ECG triggering, 120 kVp tube voltage, 80 mAs reference tube current, 0.25 seconds gantry rotation time, and 2 x 192 x 0.6 mm collimation.

2) A UHP ECG-gated spiral acquisition with Sn150 kVp tube voltage, 180 mAs reference tube current, 0.25 seconds gantry rotation time, and 2 x 192 x 0.6 mm detector collimation with a pitch of 3.2.

Automated tube current modulation (CAREDose 4D, Siemens Healthineers) was turned on for both acquisitions. The radiation exposure was recorded as CT dose index volume ($CTDI_{vol}$) and dose length product (DLP) provided by the scanner. The radiation effective dose (ED) was calculated using a cardiac-specific conversion factor of 0.026 mSv x mGy^{-1} x cm^{-1}, as shown in equation [17]:

$$ED\ (mSv) = DLP\ (mGy \times cm) \times 0.026\ (mSv \times mGy^{-1} \times cm^{-1})$$

Two reconstruction algorithms were used for image reconstruction. Both standard 120 kVp acquisitions and UHP Sn150 kVp acquisitions were reconstructed using the standard Qr36d kernel. In addition, UHP Sn150 kVp acquisitions were reconstructed using a kVp-independent algorithm (Recon CT 14.2.0, Siemens Healthineers). The algorithm includes a voltage-dependent look-up table. Using a delegated Sa36d kernel, the algorithm could generate images at any kVps with calcium Hounsfield unit (HU) values equivalent to that at 120 kVp, which minimizes the dependence of Agatston scores on tube voltage [16].

Thus, each patient had three datasets acquired from two

https://doi.org/10.3348/kjr.2021.0050

Korean Journal of Radiology
KJR

scans: protocol A (120 kVp + Qr36d), protocol B (Sn150 kVp + Qr36d), and protocol C (Sn150 kVp + Sa36d). All images were reconstructed with a 3.0-mm section thickness with an increment of 3.0 mm.

Agatston Score Assessments and Objective and Subjective Analyses

One radiologist (with 14 years of experience), blinded to the acquisition protocols and patient information, interpreted the CACS datasets of all patients. Calcification was defined as plaque covering an area of 1.03 mm^2 determined with a detection threshold of 130 HU [1]. The Agatston scores were categorized into four based on the results derived from protocol A used as the reference value [18-23]: 1) non-identifiable disease group, Agatston score = 0, 2) mild disease group, Agatston score = 1–99, 3) moderate group, Agatston score = 100–300, and 4) severe group, Agatston score > 300. The Agatston score for the UHP Sn150 kVp mode was compared with that for the standard 120 kVp mode. A radiologist also rated the overall dataset image quality from protocols A and C using a 5-point Likert scale, as previously described [14]. The scale was interpreted as follows: 1 as non-diagnostic, due to the presence of severe image noise and artifacts, 2 as poor diagnostic with image noise and artifacts, 3 as fairly diagnostic with moderate image quality, 4 as diagnostic, defined as good image quality with minimal image noise and artifacts, and 5 as diagnostic, with excellent image quality. For each patient, a 1-cm^2 region of interest (ROI) was placed at the root of the aorta. Consistent ROI placement and size during all examinations were ensured using the copy-paste function of the evaluation software (Syngo.via, version VB20, Siemens Healthineers). The standard deviation of the CT attenuation for the ROI was defined as the image noise. The CT value, image noise, and signal-to-noise ratios (SNRs, defined as CT values of ROIs divided by the standard deviations of the ROI) were recorded.

Sample Size Calculation

The sample size estimation was performed using the MedCalc software (version 16.8). As no previous publication exists regarding the new algorithm with UHP using Sn150 kVp, we determined the sample size based on 15 preliminary results in our institute (not the current cohort). We set the expected mean difference as 10, the expected standard deviation of the difference to 25, and the maximum allowed difference as 72 in the software. A total of 90 participants were required to achieve 80% power to reject the null hypothesis at a two-sided significance level of 0.05. A total of 114 participants were enrolled in our study, which provided a power of > 80%.

Statistical Analyses

The statistical analyses were performed using IBM SPSS Statistics for Windows, version 25.0. (IBM Corp.) and R software (https://www.r-project.org/). Normal distributions were assessed using the Shapiro–Wilk test. Normally distributed variables are expressed as mean ± standard deviation, whereas non-normally distributed variables are reported as medians with interquartile ranges (IQRs). Student's *t* test was used to analyze the normally distributed data, and the Mann–Whitney U test was used to analyze skewed data. The categorical variables were reported as counts (%) and compared using Fisher's exact test or chi-squared test, according to the data cell sizes. The inter-technology agreement of the Agatston score for all patients using the three protocols was examined using two–way, mixed, and consistency intraclass correlation coefficients (ICCs). Inter-technology agreement of risk stratification was assessed using linear weighted kappa analyses. Bland–Altman analyses were performed to evaluate the differences among the Agatston scores derived from three datasets, and scatter plots were used to show the inter-technology delta (Δ) Agatston score tendency as calcification increased. The correlation between protocols A and C was assessed using Spearman's rank correlation coefficient. Statistical significance was set at $p < 0.05$.

RESULTS

Patient Characteristics

The mean heart rate and body mass index (BMI) of the 114 patients were 62.5 ± 5.2 bpm and 25.0 ± 2.7 kg/m^2, respectively. The patient demographics and baseline characteristics are presented in Table 1.

Agatston Score and Risk Stratification

No significant differences in the Agatston score were observed between protocols A and C (median 63.05 [IQR, 0–232.28] vs. median 60.25 [IQR, 0–195.20], $p = 0.060$) (Fig. 1). For protocol B, the Agatston score, compared with protocol A, was significantly underestimated (median, 34.85; IQR, 0–120.73; $p < 0.001$) (Fig. 1). The ICC of

 https://doi.org/10.3348/kjr.2021.0050

Table 1. Patient Characteristics

Factor	Value
Age, year	60.3 ± 9.8
Male	74 (64.9)
Heart rate, beats/min	62.5 ± 5.2
BMI, kg/m^2	25.0 ± 2.7
Hypertension	44 (38.6)
Dyslipidemia	77 (67.5)
Diabetes	22 (19.3)
Family History of CAD	54 (47.4)

Data are presented as mean ± standard deviation or number of patients with the percentage in parentheses. BMI = body mass index, CAD = coronary artery disease

the Agatston scores for protocols A and B was 0.947 (95% confidence interval [CI]: 0.924–0.963), and it was 0.997 (95% CI: 0.996–0.998) for protocols A and C. A representative case is shown in Figure 2.

The Bland–Altman plot showed that the mean difference between the Agatston score values obtained from protocols A and C was -7.82 (95% limits of agreement, -65.20 to 49.56), whereas the mean difference between protocols A and B was -73.45 (95% limits of agreement, -264.55 to 137.64) (Fig. 3A, B). An excellent correlation was also found between the Agatston scores for protocols A and C, as shown in Figure 3C.

The patients were divided into no identifiable (n = 33),

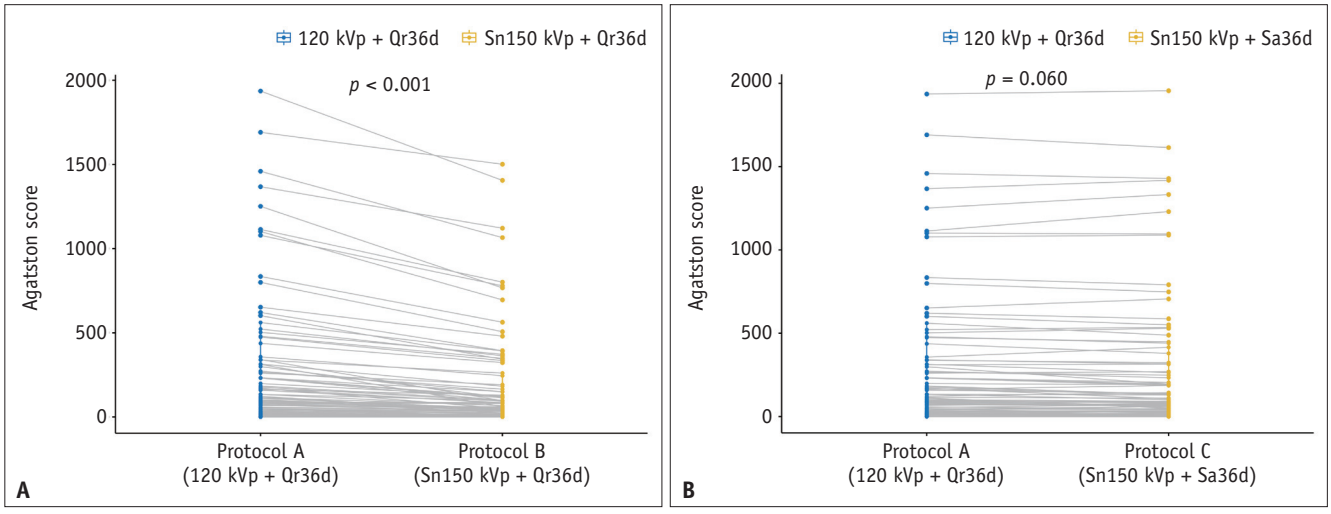

Fig. 1. Ladder plots show the Agatston scoring comparison.
A, B. Agatston scoring for protocol A compared with those for protocol B **(A)** and protocol C **(B)**.

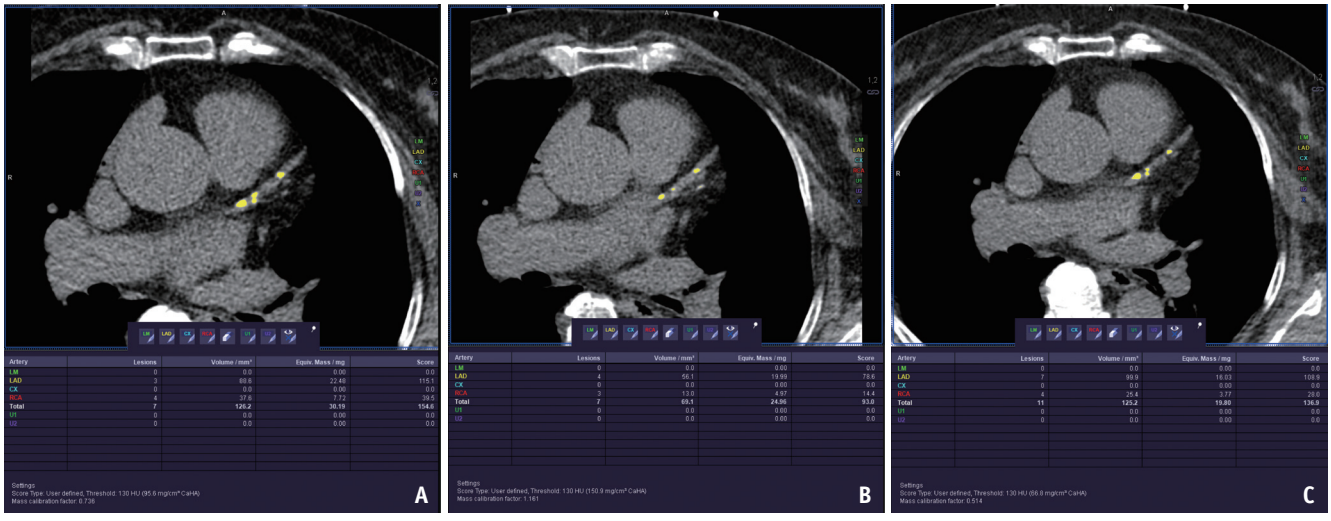

Fig. 2. A representative case of Agatston scores using protocols B and C. The patient was a 71-year-old female.
A. The Agatston score for protocol A showed a total score of 154.6. **B.** The Agatston score for protocol B shows an underestimation to 93.0 due to a lower CT value, which led to an incorrect classification of the risk category. **C.** Agatston score for protocol C after CT value correction. The calculated Agatston score of 136.9 remained comparable to that for protocol A.

https://doi.org/10.3348/kjr.2021.0050

Korean Journal of Radiology
KJR

mild (n = 34), moderate (n = 23), and severe disease (n = 24) using the standard 120 kVp protocol. The underestimation of the Agatston score for protocol B was observed in the mild, moderate, and severe groups. In contrast, protocol C achieved a correct estimation of the Agatston score in these groups. For the mild-risk group, the mean difference was -18.94 (95% limits of agreement, -50.08 to 12.19) for protocols A and B and -1.97 (95% limits of agreement, -24.75 to 20.81) for protocols A and C. For the moderate-risk group, the mean difference was -86.13 (95% limits of agreement, -153.33 to -18.94) for protocols A and B and -29.86 (95% limits of agreement, -87.73 to 28.01) for protocols A and C. For the severe-risk group, the mean difference was -239.52 (95% limits of agreement, -474.97 to -4.08) for protocols A and B and -5.73 (95% limits of agreement, -104.80 to 93.34) for protocols A and C. An underestimation tendency was observed for protocol B as calcification increased, whereas protocol C remained stable (Fig. 4).

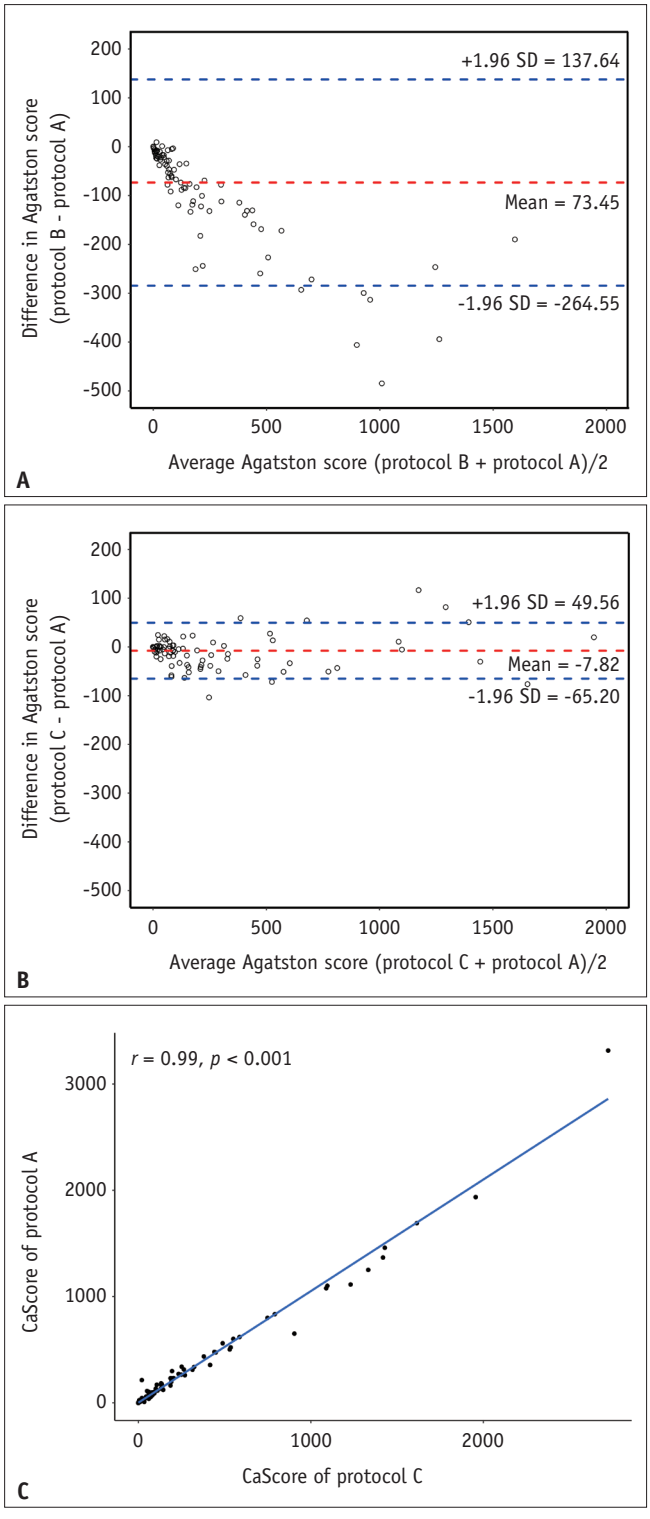

Fig. 3. Agreement and correlation among protocols.
A. Bland–Altman plot for protocols A and B. **B.** Bland–Altman plot for protocols A and C. **C.** Scatter plot shows an excellent correlation between protocols A and C, with $r = 0.99$. SD = standard deviation

There were eight outliers between protocols A and C in the Bland–Altman plot. No statistical differences in the heart rate and BMI were observed between the outlier and non-outlier patients (heart rate: 59.9 ± 6.0 bpm vs. 64.2 ± 11.2 bpm, $p = 0.145$; BMI: 26.1 ± 2.5 kg/m^2 vs. 25.0 ± 2.7 kg/m^2, $p = 0.218$). Seven out of eight outliers were from the severe-risk group and the remaining one was from the moderate-risk group. The outlier group had more severe patients with an Agatston score of 882.85 (IQR, 509.73–1280.25) than the non-outlier group, with an Agatston score of 46.05 [IQR, 0–175.53]; $p < 0.001$). A representative patient is shown in Supplementary Figure 1. Excluding one

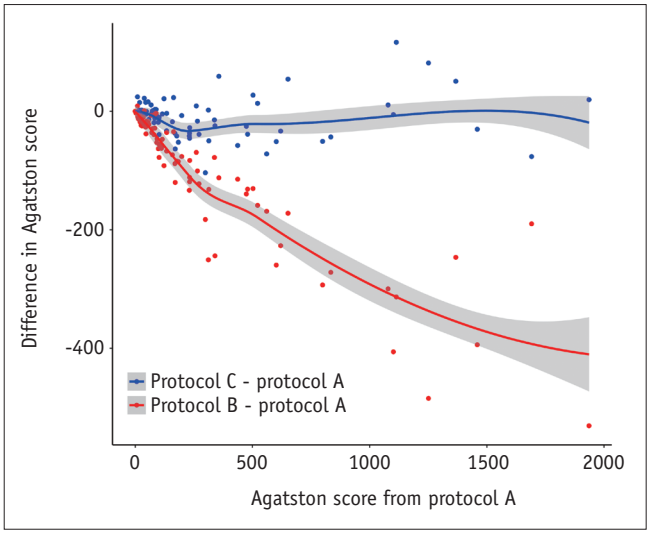

Fig. 4. Scatter plot shows the difference in the Agatston score as calcification increases. The blue line indicates that the difference in the Agatston score using the Sa36d kernel is stable, whereas the red line shows that using the Qr36d kernel results in an underestimation as calcification increases.

https://doi.org/10.3348/kjr.2021.0050

Table 2. Patient Reclassification for Protocols B and C

Protocol A Classification	Protocol C Classification			
	No	Mild	Moderate	Severe
No	33	0	0	0
Mild	0	34	0	0
Moderate	0	4	19	0
Severe	0	0	1	23
kappa	0.96 (95% confidence interval: 0.93–1.00)			
Protocol A Classification	Protocol B Classification			
	No	Mild	Moderate	Severe
No	33	0	0	0
Mild	1	33	0	0
Moderate	0	14	9	0
Severe	0	2	7	15
kappa	0.80 (95% confidence interval: 0.73–0.88)			

outlier with suboptimal image quality (subjective score, 3% difference, -34.68%), the percent difference ranged from -12.82% to 16.56%. None of the patients was misclassified.

Regarding risk stratifications, 109 of 114 (95.61%) patients were correctly identified using protocol C, whereas protocol B only identified 90 of 114 (78.95%) patients. For the non-identifiable disease group, all patients were correctly classified using both protocols. Protocol C demonstrated superiority in performance at risk classification to protocol B. Nineteen patients were reclassified using protocol C.

As shown in Table 2, when compared with protocol A, protocol C had a higher weighted kappa value (0.96; 95% CI, 0.93–1.00) than protocol B (0.80; 95% CI, 0.73–0.88). Five patients who were classified into a different risk category by protocol C did not show a higher BMI (median, 24.4 kg/m^2; IQR, 23.1–27.1) than the concordant cases (median, 24.9 kg/m^2; IQR, 23.4–26.7; p = 0.800) or a higher heart rate (median 63 [IQR, 56–77] vs. median 62 [IQR, 57–68], p = 0.590).

Image Quality Assessments

The CT values (median 43.5 HU vs. 44.0 HU), image noises (both 14 HU), and SNR (3.113 vs. 3.143) showed no significant differences for protocols A and C (all p > 0.05). Subjective image quality assessment also showed comparable performances of protocols A and C (Table 3).

Dose Comparison

Protocols B and C used the same parameters for CT scan acquisition; therefore, their radiation doses were the same. Compared with the standard ECG-triggered mode (protocol A), the UHP mode (protocols B and C) significantly reduced the radiation dose in terms of $CTDI_{vol}$ (1.35 mGy vs. 2.51 mGy, p < 0.001), DLP (22.1 mGy x cm vs. 31.6 mGy x cm, p < 0.001), and ED (0.58 mSv vs. 0.82 mSv, p < 0.001). ED was reduced by approximately 30% (Table 3).

Table 3. Comparisons between Protocols A and C according to the Radiation Dose and Image Quality

	Protocol A	Protocol C	*P*
Image quality			
CT value, HU	43.5 (40, 46)	44 (41, 45)	0.370
Noise, HU	14 (12, 17)	14 (13, 17)	0.859
SNR	3.11 (2.76, 3.49)	3.14 (2.58, 3.44)	0.869
Subjective rate	5 (4, 5)	5 (4, 5)	0.735
Dose			
Scan mode	Standard 120 kVp mode	UHP Sn150 kVp mode	
$CTDI_{vol}$, mGy	2.51 (2.13, 2.86)	1.35 (1.22, 1.47)	< 0.001
DLP, mGy x cm	31.6 (27.53, 35.95)	22.1 (20.43, 24.10)	< 0.001
ED, k = 0.026	0.82 (0.72, 0.94)	0.58 (0.53, 0.63)	< 0.001

Data are presented as median (interquartile range). $CTDI_{vol}$ = volumetric CT dose index, DLP = dose-length-product, ED = effective dose, HU = Hounsfield unit, SNR = signal-to-noise ratio, UHP = ultra-high-pitch

DISCUSSION

In this study, the Agatston score for the UHP Sn150 kVp acquisitions using the Sa36d kernel showed excellent agreement and correlation with the standard 120 kVp acquisition mode using the standard reconstruction algorithm. The Agatston score and risk stratification for the UHP Sn150 kVp acquisitions using the standard algorithm showed an underestimation and was improved by the kVp-independent algorithm. The improvement was observed especially in patients with Agatston scores ranging from 100 to 300 and greater than 300. In addition, the UHP Sn150 kVp acquisitions allowed for a 30% reduction in the radiation dose without affecting the overall image quality, compared with the standard 120 kVp mode.

CACS has been proven to be an important risk stratification factor in patients with coronary artery disease and plays an essential role in disease monitoring [24,25]. The radiation dose from CACS scanning has decreased in recent years and now falls within the range of 1–1.5 mSv in daily clinical practice [26]. Due to the increasing demand for CT examinations to obtain CACS, any further reduction of radiation exposure may lead to a reduced radiation-related risk not only on one patient but also at a population level

https://doi.org/10.3348/kjr.2021.0050

Korean Journal of Radiology
KJR

while following the "as-low-as-reasonably-achievable" principle [9]. The implementation of a low-dose protocol could lead to higher noise and, ultimately, result in an inaccurate Agatston score. Our study attempted to use two technologies, UHP and spectral shaping, to achieve this goal while maintaining the Agatston score accuracy by introducing a novel reconstruction algorithm.

Previous studies have investigated whether the UHP acquisition mode could reduce the radiation dose while maintaining imaging accuracy [27-29]. With a sample size of 1000 patients, Xia et al. [29] found that the Agatston score was significantly lower in the 120 kVp non-gated high-pitch chest CT mode than that on cardiac CT, and the median percentage difference in CACS was 29% (range, 0%–200%). We also found that using the standard Qr36d kernel in UHP mode with Sn150 kVp resulted in a CACS underestimation as compared with the standard 120 kVp mode. However, by using the kVp-independent algorithm, similar Agatston scores can be achieved in UHP Sn150 kVp acquisition as compared to the standard 120 kVp mode.

Tin filter technology is often combined with UHP to further reduce the radiation dose. For spectral-shaping technology, a tin filter is positioned in front of the X-ray tube radiation exit window, leading to narrower X-ray tube spectra with fewer quanta at lower energies. Spectral changes result in the modification of CT values, thus impacting the accuracy of the Agatston score. Apfaltrer et al. [10] found that the Agatston score from the Sn100 kVp protocol was overestimated (34.9% vs. 41.7%, $p < 0.001$), although the CACS risk category was not affected. Marwan et al. [6] also demonstrated that CACS threshold adjustments should be implemented to maintain consistent Agatston scores while using UHP Sn100 kVp scan modes. Usually, the UHP mode achieves a dose reduction of 60%–70% [10-12] compared with the standard protocol when Sn100 kVp is used. However, their results may suggest an underestimation of the Agatston score or the use of a new threshold. To obtain a more accurate CACS, ECG-triggered UHP mode with Sn150 kVp was used in this study, which may limit the potential for dose reduction. This is the first step in investigating the accuracy of the algorithm under the UHP mode. Further studies can be carried out to investigate the strategies for dose reduction using a lower kVp protocol setting or non-ECG-gated mode. The Sa36d kernel, which is independent of the tube voltage, was used to improve the inaccurate estimation of the Agatston score for different tube voltage settings [16]. With a prospective ECG-triggered mode, a strong agreement of the Agatston scores for Sn100 kVp or patient-adapted kVp using this algorithm and the standard protocol was observed [15,16]. In this study, we focused on determining whether the Sa36d reconstruction algorithm could also maintain CACS accuracy using the UHP Sn150 kVp mode. No statistical differences were observed, although the underestimation of CACS still exists. Therefore, a low-dose CACS scan can be directly interpreted without threshold modifications.

We also observed several outliers in the Bland–Altman plot, with the majority occurring in the severe-risk group. This indicates that the acquired Agatston score difference between the UHP Sn150 kVp and standard 120 kVp modes was enlarged in the severe calcification case, even when the correction algorithm was applied to the images. Nevertheless, the relative difference remained acceptable and did not alter risk classification. Additionally, the Agatston score calculation does not use a continuous equation. Four weights were identified based on the CT value range [1]: 1, 130–199; 2, 200–299; 3, 300–399; and 4, ≥ 400. The Agatston score sums up the product of the area and weight for all the CT value ranges. These outliers have suboptimal image quality, and the CT value may not be sufficiently accurate to obtain the same weight as in the standard mode.

Since the pitch was largely augmented and the radiation dose of the Sn150 kVp acquisitions was significantly reduced, which may have affected the image quality, we also performed subjective and objective assessments. For subjective assessments, visual rankings were clinically feasible for the Sa36d kernel dataset (median: level 4). For objective measurements, no significant differences in attenuation, noise, and SNR were observed. Several studies have shown that the image quality of the UHP mode is comparable to that of the standard modes [30,31]. The improvement in ICC in our results indicated that the Sa36d kernel applied in protocol C effectively preserved the Agatston score accuracy as compared with the standard 120 kVp mode. The absolute value of dose reduction is limited (0.8 mSv vs. 0.6 mSv).

This study has several limitations. First, only patients with regular heart rates (< 75 bpm) were included in this study to ensure that the scan results were interpretable. This limitation should be carefully considered during the implementation of UHP modes in the future. Second, this was a single-center study with a relatively small sample. A larger cohort is needed to validate our results. Third, only

 https://doi.org/10.3348/kjr.2021.0050

one radiologist performed the quantitative and qualitative analyses. No interobserver results were obtained. However, the measurement of CACS is routine for clinicians. We assume that these results are reliable and reproducible. Finally, the UHP scan mode, tin filter technology, and new Sa36d reconstruction algorithm are only available for some systems from one vendor, which may impact the generalization of our results.

In conclusion, CACS based on UHP Sn150 kVp acquisitions with a kVp-independent reconstruction algorithm demonstrated excellent agreement with that based on the standard 120 kVp acquisitions, as shown by the Agatston score and risk categorization. The new algorithm also allowed a significant decrease in radiation dose.

Supplement

The Supplement is available with this article at https://doi.org/10.3348/kjr.2021.0050.

Conflicts of Interest

Xinwei Tao is an employee of Siemens Healthineers China. Thomas Allmendinger is an employee of Siemens Healthcare, Forchheim, Germany. All other authors declare no conflicts of interest.

Author Contributions

Conceptualization: Xi Hu, Zhongfeng Niu, Bin Chen. Data curation: Xi Hu, Yueqiao Zhang, Yong Zhang. Formal analysis: Xi Hu, Yueqiao Zhang, Bin Chen. Funding acquisition: Zhongfeng Niu, Bin Chen. Investigation: Xi Hu, Xinwei Tao, Zhongfeng Niu, Yong Zhang. Methodology: Thomas Allmendinger, Yu Kuang. Project administration: Xi Hu, Zhongfeng Niu, Yu Kuang. Resources: Xi Hu, Yueqiao Zhang, Yu Kuang, Bin Chen. Software: Xinwei Tao, Thomas Allmendinger. Supervision: Yu Kuang, Bin Chen. Validation: Xi Hu, Xinwei Tao, Zhongfeng Niu. Visualization: Xinwei Tao, Zhongfeng Niu. Writing—original draft: Xi Hu, Xinwei Tao. Writing—review & editing: Yu Kuang, Bin Chen.

ORCID iDs

Xi Hu
https://orcid.org/0000-0002-6485-8837
Xinwei Tao
https://orcid.org/0000-0002-1421-3846
Yueqiao Zhang
https://orcid.org/0000-0002-0356-1917
Zhongfeng Niu
https://orcid.org/0000-0001-7283-8257
Yong Zhang
https://orcid.org/0000-0003-1777-788X
Thomas Allmendinger
https://orcid.org/0000-0002-3133-4017
Yu Kuang
https://orcid.org/0000-0001-9451-4640
Bin Chen
https://orcid.org/0000-0002-8167-9101

REFERENCES

1. Agatston AS, Janowitz WR, Hildner FJ, Zusmer NR, Viamonte M Jr, Detrano R. Quantification of coronary artery calcium using ultrafast computed tomography. *J Am Coll Cardiol* 1990;15:827-832
2. Baron KB, Choi AD, Chen MY. Low radiation dose calcium scoring: evidence and techniques. *Curr Cardiovasc Imaging Rep* 2016;9:12
3. Bittencourt MS, Blaha MJ, Blankstein R, Budoff M, Vargas JD, Blumenthal RS, et al. Polypill therapy, subclinical atherosclerosis, and cardiovascular events-implications for the use of preventive pharmacotherapy: MESA (multi-ethnic study of atherosclerosis). *J Am Coll Cardiol* 2014;63:434-443
4. Darabian S, Luo Y, Homat A, Khosraviani K, Wong N, Zeb I, et al. CAC score as a possible criterion for administration of angiotensin converting enzyme inhibitors and/or angiotensin receptor blockers: the MultiEthnic Study of Atherosclerosis. *Coron Artery Dis* 2015;26:678-685
5. Hecht HS, Cronin P, Blaha MJ, Budoff MJ, Kazerooni EA, Narula J, et al. 2016 SCCT/STR guidelines for coronary artery calcium scoring of noncontrast noncardiac chest CT scans: a report of the Society of Cardiovascular Computed Tomography and Society of Thoracic Radiology. *J Cardiovasc Comput Tomogr* 2017;11:74-84
6. Marwan M, Mettin C, Pflederer T, Seltmann M, Schuhbäck A, Muschiol G, et al. Very low-dose coronary artery calcium scanning with high-pitch spiral acquisition mode: comparison between 120-kV and 100-kV tube voltage protocols. *J Cardiovasc Comput Tomogr* 2013;7:32-38
7. Voros S, Rivera JJ, Berman DS, Blankstein R, Budoff MJ, Cury RC, et al. Guideline for minimizing radiation exposure during acquisition of coronary artery calcium scans with the use of multidetector computed tomography: a report by the Society for Atherosclerosis Imaging and Prevention Tomographic Imaging and Prevention Councils in collaboration with the Society of Cardiovascular Computed Tomography. *J Cardiovasc Comput Tomogr* 2011;5:75-83
8. Kamani CH, Huang W, Lutz J, Giannopoulos AA, Patriki D, von Felten E, et al. Impact of adaptive statistical iterative reconstruction-V on coronary artery calcium scores obtained

from low-tube-voltage computed tomography - A patient study. *Acad Radiol* 2020:S1076-6332(20)30613-30619
9. Gräni C, Vontobel J, Benz DC, Bacanovic S, Giannopoulos AA, Messerli M, et al. Ultra-low-dose coronary artery calcium scoring using novel scoring thresholds for low tube voltage protocols-a pilot study. *Eur Heart J Cardiovasc Imaging* 2018;19:1362-1371
10. Apfaltrer G, Albrecht MH, Schoepf UJ, Duguay TM, De Cecco CN, Nance JW, et al. High-pitch low-voltage CT coronary artery calcium scoring with tin filtration: accuracy and radiation dose reduction. *Eur Radiol* 2018;28:3097-3104
11. McQuiston AD, Muscogiuri G, Schoepf UJ, Meinel FG, Canstein C, Varga-Szemes A, et al. Approaches to ultra-low radiation dose coronary artery calcium scoring based on 3rd generation dual-source CT: a phantom study. *Eur J Radiol* 2016;85:39-47
12. Vonder M, Pelgrim GJ, Huijsse SE, Meyer M, Greuter MJ, Henzler T, et al. Feasibility of spectral shaping for detection and quantification of coronary calcifications in ultra-low dose CT. *Eur Radiol* 2017;27:2047-2054
13. Hecht HS, de Siqueira ME, Cham M, Yip R, Narula J, Henschke C, et al. Low- vs. standard-dose coronary artery calcium scanning. *Eur Heart J Cardiovasc Imaging* 2015;16:358-363
14. Tesche C, De Cecco CN, Vliegenthart R, Albrecht MH, Varga-Szemes A, Duguay TM, et al. Accuracy and radiation dose reduction using low-voltage computed tomography coronary artery calcium scoring with tin filtration. *Am J Cardiol* 2017;119:675-680
15. Vingiani V, Abadia AF, Schoepf UJ, Fischer AM, Varga-Szemes A, Sahbaee P, et al. Low-kV coronary artery calcium scoring with tin filtration using a kV-independent reconstruction algorithm. *J Cardiovasc Comput Tomogr* 2020;14:246-250
16. Vingiani V, Abadia AF, Schoepf UJ, Fischer AM, Varga-Szemes A, Sahbaee P, et al. Individualized coronary calcium scoring at any tube voltage using a kV-independent reconstruction algorithm. *Eur Radiol* 2020;30:5834-5840
17. Trattner S, Halliburton S, Thompson CM, Xu Y, Chelliah A, Jambawalikar SR, et al. Cardiac-specific conversion factors to estimate radiation effective dose from dose-length product in computed tomography. *JACC Cardiovasc Imaging* 2018;11:64-74
18. Budoff M, Backlund JC, Bluemke DA, Polak J, Bebu I, Schade D, et al. The association of coronary artery calcification with subsequent incidence of cardiovascular disease in type 1 diabetes: the DCCT/EDIC trials. *JACC Cardiovasc Imaging* 2019;12:1341-1349
19. Budoff MJ, Young R, Burke G, Jeffrey Carr J, Detrano RC, Folsom AR, et al. Ten-year association of coronary artery calcium with atherosclerotic cardiovascular disease (ASCVD) events: the multi-ethnic study of atherosclerosis (MESA). *Eur Heart J* 2018;39:2401-2408
20. Hecht HS, Blaha MJ, Kazerooni EA, Cury RC, Budoff M, Leipsic J, et al. CAC-DRS: coronary artery calcium data and reporting system. An expert consensus document of the society of cardiovascular computed tomography (SCCT). *J Cardiovasc Comput Tomogr* 2018;12:185-191
21. Madder RD, VanOosterhout S, Klungle D, Mulder A, Elmore M, Decker JM, et al. Multimodality intracoronary imaging with near-infrared spectroscopy and intravascular ultrasound in asymptomatic individuals with high calcium scores. *Circ Cardiovasc Imaging* 2017;10:e006282
22. Merghani A, Maestrini V, Rosmini S, Cox AT, Dhutia H, Bastiaenan R, et al. Prevalence of subclinical coronary artery disease in masters endurance athletes with a low atherosclerotic risk profile. *Circulation* 2017;136:126-137
23. Silverman MG, Blaha MJ, Krumholz HM, Budoff MJ, Blankstein R, Sibley CT, et al. Impact of coronary artery calcium on coronary heart disease events in individuals at the extremes of traditional risk factor burden: the Multi-Ethnic Study of Atherosclerosis. *Eur Heart J* 2014;35:2232-2241
24. Mitchell JD, Fergestrom N, Gage BF, Paisley R, Moon P, Novak E, et al. Impact of statins on cardiovascular outcomes following coronary artery calcium scoring. *J Am Coll Cardiol* 2018;72:3233-3242
25. Lee SE, Sung JM, Andreini D, Budoff MJ, Cademartiri F, Chinnaiyan K, et al. Differential association between the progression of coronary artery calcium score and coronary plaque volume progression according to statins: the Progression of AtheRosclerotic PlAque DetermIned by Computed TomoGraphic Angiography Imaging (PARADIGM) study. *Eur Heart J Cardiovasc Imaging* 2019;20:1307-1314
26. Nieman K. Evolve or perish for coronary calcium imaging. *Eur Heart J Cardiovasc Imaging* 2015;16:354-355
27. Vonder M, Vliegenthart R, Kaatee MA, van der Aalst CM, van Ooijen PMA, de Bock GH, et al. High-pitch versus sequential mode for coronary calcium in individuals with a high heart rate: potential for dose reduction. *J Cardiovasc Comput Tomogr* 2018;12:298-304
28. Ochs MM, Andre F, Korosoglou G, Fritz T, Seitz S, Bogomazov Y, et al. Strengths and limitations of coronary angiography with turbo high-pitch third-generation dual-source CT. *Clin Radiol* 2017;72:739-744
29. Xia C, Vonder M, Pelgrim GJ, Rook M, Xie X, Alsurayhi A, et al. High-pitch dual-source CT for coronary artery calcium scoring: a head-to-head comparison of non-triggered chest versus triggered cardiac acquisition. *J Cardiovasc Comput Tomogr* 2021;15:65-72
30. Aksoy EA, Özden SU, Karaarslan E, Ünal ÖF, Tanyeri H. Reliability of high-pitch ultra-low-dose paranasal sinus computed tomography for evaluating paranasal sinus anatomy and sinus disease. *J Craniofac Surg* 2014;25:1801-1804
31. Leyendecker P, Faucher V, Labani A, Noblet V, Lefebvre F, Magotteaux P, et al. Prospective evaluation of ultra-low-dose contrast-enhanced 100-kV abdominal computed tomography with tin filter: effect on radiation dose reduction and image quality with a third-generation dual-source CT system. *Eur Radiol* 2019;29:2107-2116